Journal of Remote Sensing
A SCIENCE PARTNER JOURNAL

RESEARCH ARTICLE

A Novel Hyperspectral Remote Sensing Technique with Hour-Hectometer Level Horizontal Distribution of Trace Gases: To Accurately Identify Emission Sources

Chuan Lu[1,2], Qihua Li[3*], Chengzhi Xing[1], Qihou Hu[1], Wei Tan[1], Hua Lin[1,2], Jinan Lin[1,2], Zhiguo Zhang[2], Bowen Chang[3], and Cheng Liu[2,4,5*]

[1]Key Lab of Environmental Optics & Technology, Anhui Institute of Optics and Fine Mechanics, Hefei Institutes of Physical Science, Chinese Academy of Sciences, Hefei 230031, China. [2]Department of Precision Machinery and Precision Instrumentation, University of Science and Technology of China, Hefei 230026, China. [3]Institutes of Physical Science and Information Technology, Anhui University, Hefei 230039, China. [4]Key Laboratory of Precision Scientific Instrumentation of Anhui Higher Education Institutes, University of Science and Technology of China, Hefei 230026, China. [5]Anhui Province Key Laboratory of Polar Environment and Global Change, University of Science and Technology of China, Hefei 230026, China.

*Address correspondence to: chliu81@ustc.edu.cn (C.L.); lqh628@ahu.edu.cn (Q.L.)

Citation: Lu C, Li Q, Xing C, Hu Q, Tan W, Lin H, Lin J, Zhang Z, Chang B, Liu C. A Novel Hyperspectral Remote Sensing Technique with Hour-Hectometer Level Horizontal Distribution of Trace Gases: To Accurately Identify Emission Sources. *J. Remote Sens.* 2023;3:Article 0098. https://doi.org/10.34133/remotesensing.0098

Submitted 31 March 2023
Accepted 24 October 2023
Published 14 November 2023

High spatial-temporal resolution distribution of atmospheric gaseous pollutant is an important basis for tracing its emission, transport, and transformation. Typical methods for acquiring regional atmospheric gaseous pollutant distributions are satellite remote sensing and in situ observations. However, these approaches have limitations, such as sparse overpass times for satellites and restricted coverage for in situ monitoring. In this study, we propose a method for the long-term detection of the horizontal distribution of trace gases. This method based on effective optical paths (EOPs) as the instrument's detection range. It acquires the average trace gas concentration along the EOPs by utilizing different detection distances within the ultraviolet (UV) and visible (VIS) spectral bands. Subsequently, we use the onion-peeling method to obtain trace gas concentrations at two distinct distances. The obtained trace gas horizontal distribution was consistent with the in situ and mobile measurements. Compared with satellite remote sensing, this method achieved horizontal distribution results with higher spatial and temporal resolutions, and located several small high-value areas in Hefei, China. The tropospheric NO_2 vertical column density (VCD) results of the satellite at transit time (13:30) were consistent with the hyperspectral NO_2 horizontal distribution results at 13:00 to 14:00 on the same day but were not consistent with the daily average NO_2 results. The hourly NO_2 concentration in each area was 10% to 40% lower than the daytime average obtained by the hyperspectral remote sensing result. We evaluated the errors associated with the calculation of NO_2 emissions based on the satellite results and found a bias of approximately 69.45% to 83.34%. The spatial distribution of NO_2 concentration obtained from MAX-DOAS measurements may help in future bottom-up emission calculations.

Introduction

The rapid development of China's economy and urbanization has led to considerable air pollution, particularly in cities [1]. Among them, nitrogen dioxide (NO_2) is one of the most important ambient air pollutants [2]. Anthropogenic sources of emissions from industry, transportation, and biomass combustion have substantially increased the near-surface concentrations of NO_2 gases, causing environmental effects, including acid rain, seriously damaging the ecological balance [3]. NO_2 is an important precursor that contributes considerably to the formation of secondary aerosols and ozone in the atmosphere [4], which can influence the surface energy balance and climate change [5,6]. The long-term exposure of humans to high concentrations of NO_2 can cause respiratory damage and worsen the symptoms of bronchitis [7]. However, urban car emissions change spatially and temporally, as do NO_2 concentrations, rendering them extremely heterogeneous [8]. Therefore, obtaining horizontal distribution changes in NO_2 concentrations in urban areas can improve our understanding of regional air pollution transmission and help protect the health of residents.

The horizontal distribution of NO_2 is widely used in pollutant flux and emission inventory calculations, as well as hotspot identification [9]. Traditionally, the main approaches used to

monitor the regional distribution of air pollutants are in situ monitoring and satellite remote sensing [10,11]. However, the limited number of in situ monitoring devices means that urban, suburban, and rural areas are scarcely covered. On the other hand, satellite remote sensing covers large areas and has the advantage of analyzing the spatial and temporal distribution of pollutants [12]. Currently, many satellite remote sensing payloads are widely used to observe air pollutants worldwide, including GOME-2 [13], OMI [14], EMI [15], and TROPOMI [16]. Among these, TROPOMI has the highest spatial resolution of 5.5 × 3.5 km (along-track × across-track) at nadir for bands since 2019 August 6 [17].

Geosynchronous satellite tropospheric NO_2 vertical column densities (VCDs) have been widely used in bottom-up emission and regional transmission flux calculations within urban areas. The basic assumption is that the geosynchronous satellite tropospheric NO_2 VCD is equivalent to the daytime average tropospheric NO_2 VCD [18]. However, geosynchronous satellites have a sun-synchronous orbit with only a local time overpass; therefore, it is not possible to discern the daily variation of the pollutant results obtained based on satellites. Therefore, the calculation of bottom-up emissions adds additional uncertainty. The Emissions Database for Global Atmospheric Research (ver5.0, 2015) have reported that the uncertainty of NO_x emission source results ranged from 17.2% to 69.4%, and only have estimated the uncertainty on the estimated part of the emissions, not accounting for the missing super-emitting factors, such as vehicles [19].

Passive multi-axis differential optical absorption spectroscopy (MAX-DOAS) is a common remote sensing technique used to determine the distribution of atmospheric trace gases [20]. This technique is based on the Beer–Lambert law, which states that the absorption of electromagnetic radiation by matter can be used to calculate the concentration of each trace gas in the effective optical path (EOP) of the atmosphere [21]. By using the sun-scattered spectra of collected trace gases, the slant column densities (SCDs) can be retrieved using linear least-squares minimization [22]. Ground-based MAX-DOAS can retrieve the VCDs and vertical profiles of aerosols and trace gases by measuring the elevation angle spectra in multiple directions [23]. A ground-based MAX-DOAS that retrieves near-surface trace gas horizontal distributions in multi-azimuth angle directions has been developed. The MAX-DOAS spectral dataset with a fine spatial resolution partly resolves the horizontal distribution of near-surface trace gases around the measurement site [24]. In general, the MAX-DOAS observation elevation does not exceed 3° when retrieving the near-surface trace gas horizontal distribution [25]. Using tetra oxygen (O_4) SCDs at different wavelength intervals, the EOP at different wavelengths [26] and the trace gas concentration along the optical path can be obtained. Spectral information from different azimuth angles can be collected through the rotation of the telescope. Finally, the horizontal distribution of trace gas concentrations under different EOPs in each direction is calculated [27].

Here, we have conducted long-term monitoring using ground-based MAX-DOAS and have obtained the NO_2 horizontal distribution within the monitoring area based on the onion-peeling method.The NO_2 results obtained using this method achieved a higher spatial and temporal resolution compared with the satellite data and a higher spatial coverage compared with in situ measurements. The spatial resolution in the direction of rotation is up to 0.1°, while the spatial resolution along each azimuth depended on the difference in EOPs in different wavelength intervals and reaches the kilometer level. Temporal resolution of up to 1 h is achieved. With a higher spatial resolution, the method can be used to locate hotspots more accurately than satellite remote sensing. Moreover, it can also be used to evaluate the satellite results when the satellite VCD of its passing time is regarded as the daily average result.

Methodology

Instrument and observation scheme

The MAX-DOAS instrument employed in this study is the Airyx 2D SkySpec instrument (Heidelberg, Germany). It consists of three main components: two spectrometer boxes in a thermostat, a telescope box, and a computer for instrument control and data storage [28]. One spectrometer covers the ultraviolet (UV) wavelength range (296 to 409 nm), whereas the other works in the visible (VIS) region (402 to 565 nm). The spectral resolution was 0.45 nm.

The instrument is located on the roof of the meteorological tower in the meteorological administration of Anhui province at an approximate height of 100 m, longitude of 117.2396°E, and latitude of 31.8660°N (Fig. 1A). The observation period is from 2022 March 1 to 2022 May 31. These observations are divided into two observation modes. The vertical observation mode collects spectra at different elevation angles at a given azimuth of 135° (blue line in Fig. 1), while the horizontal observation mode collects the spectra of several azimuths at a fixed low elevation angle (Table 1). The vertical profile of NO_2 is obtained using the optimal estimation (OE) method [29,30]. A vertical profile is used to simulate the correction factor and verify the NO_2 concentration results obtained using the horizontal observation mode. The elevation angle sequence of the vertical mode is provided in Table 1. For the remaining azimuth angles (red lines in Fig. 1), the instrument is implemented at elevation angles of 0° (horizontal) and 90° (zenith). One complete scan of the region takes approximately 1 h.

Three nearby China National Environmental Monitoring Centers (CNEMCs) are selected for the validation of horizontal distribution, detailed information of which is provided in Table 2.

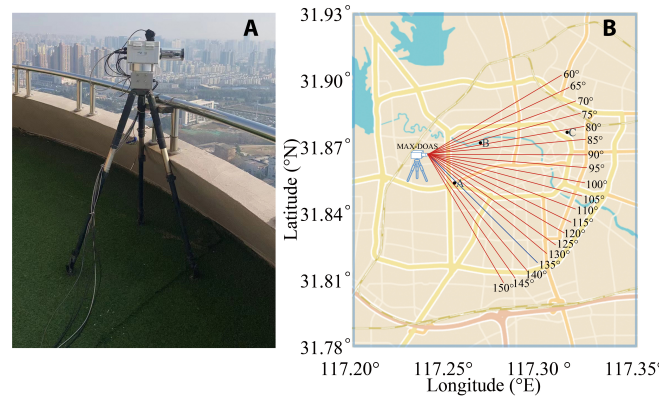

Fig. 1. (A) MAX-DOAS setup and (B) MAX-DOAS observation geometry. The black dots indicate China National Environmental Monitoring Centers (CNEMCs). Dot A: Changjiang Middle Road; dot B: Hupo Villa; dot C: Sanlijie. The blue and red lines represent the vertical profile and horizontal observations, respectively.

Table 1. The geometric setup of the MAX-DOAS measurements.

Date	Mode	Azimuth angle	Elevation angle	Total integration times for individual measurements
March 1, 2022 to May 31, 2022	Vertical	135°	0°, 1°, 2°, 3°, 4°, 5°, 8°, 10°, 15°, 30°, 90°	60 s
	Horizontal	60°, 65°, 70°, 75°, 80°, 85°, 90°, 95°, 100°, 105°, 110°, 115°, 120°, 125°, 130°, 140°, 145°, 150°	0°, 90°	60 s

Table 2. CNEMCs within the MAX-DOAS observation direction.

	Site name		
	Hupo Villa	Changjiang Middle Road	Sanlijie
Longitude	117.259°E	117.25°E	117.3070°E
Latitude	31.8706°N	31.8572°N	31.8766°N
Distance from MAX-DOAS instrument (km)	2,160 m	1,508 m	7,522 m
Azimuth relative to instrument	77.5351°	132.6141°	81.3438°

Data calculation

QDOAS software, developed by the Royal Belgian Institute for Space Aeronomy (BIRA-IASB) [31], is used to perform DOAS retrievals of aerosols and NO_2 from spectral measurements in the UV and VIS bands. A detailed algorithm and an example of the spectrum-fitting results are provided in Appendix 1 in the Supplementary Materials. Since the spectral signal may decay with time, MAX-DOAS observations with a solar zenith angle (SZA) higher than 65° are removed.

The method employed to derive the horizontal distribution of NO_2 is primarily based on the onion-peeling method. This approach is based on EOP of NO_2 in the UV and VIS spectra to calculate the NO_2 concentration in the direction of observation. QDOAS software is used to retrieve NO_2 SCDs in both the UV and VIS spectra using the method described in Appendix 1 in the Supplementary Materials. We also need to calculate the EOP length L_{NO_2}. However, the difference between the profile shapes of O_4 and NO_2 is marked. Therefore, a dimensionless correction factor f modeled by the radiative transfer model is needed to convert the O_4 optical path into the NO_2 optical path [32]:

$$L_{NO_2} = L_{O_4} \cdot f \tag{1}$$

where L_{O_4} is directly proportional to the O_4 number density, and O_4 number density is typically stable and can be calculated assuming that it is proportional to the square of O_2 [33]. O_2 is relatively constant at atmospheric density C_{air}:

$$n_{O_4} = \left(n_{O_2}\right)^2 = \left(0.20942 \cdot C_{air}\right)^2 \tag{2}$$

where n_{O_4} denotes the O_4 number density. The atmospheric density is calculated from the measured temperature T and pressure P:

$$C_{air} = \frac{\left(P \cdot N_A\right)}{\left(T \cdot R\right)} \tag{3}$$

where N_A is Avogadro's constant and R is the gas ratio constant.

The effective O_4 horizontal optical path L_{O_4} of the MAX-DOAS instrument in all directions is calculated using the following equation [34]:

$$L_{O_4} = \frac{dSCD_{mea} - dSCD_{ref}}{n_{O_4}} = \frac{dSCD_{O_4}}{n_{O_4}} \tag{4}$$

where n_{O_4} denotes the O_4 number density. The effective O_4 horizontal optical path L_{O_4} is regarded as the spatial detection range of the observation.The workflow for calculating correction factor f is provided in Appendix 2 in the Supplementary Materials. The vertical profile obtained in the vertical mode is used in modeling of the simulated NO_2 SCD by SCIATRAN. The correction factor f is the ratio of the simulated NO_2 SCD (SCD_{RTM}) to the MAX-DOAS measured NO_2 SCD ($SCD_{measured}$):

$$f = \frac{SCD_{RTM}}{SCD_{measured}} \tag{5}$$

Under a low aerosol load, the relationship between the NO_2 dSCD at a low elevation angle and near-surface concentration is as follows:

$$c_{NO_2} = \frac{dSCD_{NO_2}}{L_{NO_2}} \tag{6}$$

where c_{NO_2} is the average concentration of NO_2. Therefore, the average NO_2 concentrations of the UV and VIS optical paths are calculated. The optical path in the VIS band is always larger than that in the UV band. Therefore, the horizontal distribution in the NO_2 region is obtained using the onion-peeling method:

$$\begin{cases} c_1 = \frac{dSCD_1}{L_1} \text{ (Photon path in the UV optical path)} \\ c_2 = \frac{dSCD_2 - dSCD_1}{L_2 - L_1} \text{ (Photon path between the UV and VIS optical paths)} \end{cases} \tag{7}$$

c_2 in Eq. 7 can also be calculated as follows:

$$c_2 = \frac{c_{\text{vis}} \cdot L_2 - c_1 \cdot L_1}{L_2 - L_1} \tag{8}$$

where c_{vis} is the average concentration of the VIS optical path. Assuming that the error of concentration in the UV optical path is e_{c_1}, the cumulative error e_{c_2} of c_2 is as follows:

$$\begin{aligned} e_{c_2} = &\left|\frac{L_2}{L_2 - L_1}\right| e_{c_{\text{vis}}} + \left|\frac{L_1}{L_2 - L_1}\right| e_{c_1} \\ &+ \left|\frac{c_1 \cdot L_1 - c_{\text{vis}} \cdot L_1}{(L_2 - L_1)^2}\right| e_{L_2} + \left|\frac{c_{\text{vis}} \cdot L_2 - c_1 \cdot L_2}{(L_2 - L_1)^2}\right| e_{L_1} \end{aligned} \tag{9}$$

where $e_{c_{\text{vis}}}$ is the error of concentration c_{vis} in the VIS optical path, and the e_{L_1} and e_{L_2} are the errors of the optical paths L_1 and L_2, respectively. Evidently, e_{c_2} is larger than e_{c_1}.Due to the current need for MAX-DOAS instruments to operate in a low-elevation angle observation mode, the algorithms are closely tied to the UV-VIS path length. The UV optical path is generally shorter than the VIS optical path. Therefore, under adverse weather conditions or in areas with limited visibility, it may not be able to obtain optimal results. During study period and under favorable weather conditions, our MAX-DOAS instrument typically observed that UV EOPs mainly varies from 5 to 7 km, while VIS EOPs generally varies from 7.5 to 9.5 km.

The onion-peeling method is used to obtain the near-surface concentrations of NO_2 based on MAX-DOAS, followed by comparison with the results obtained using in situ measurements, TROPOMI VCD, and mobile DOAS. Detailed information on the mobile MAX-DOAS and Sentinel-5 satellite results is provided in Appendix 3 in the Supplementary Materials.

Results and Discussion

Validations

Two CNEMCs (Hupo Villa and Changjiang Middle Road) are closed to the MAX-DOAS instrument (<3 km). Furthermore, both of these sites are within the MAX-DOAS instrument UV EOP under load conditions. By contrast, the other site (Sanlijie) is far from the MAX-DOAS location (>7 km), beyond the MAX-DOAS UV EOP but within the VIS EOP. Thus, we have verified the NO_2 concentration results of the MAX-DOAS instrument using the UV EOP method within the two CNEMCs. We select the spectral data on no-rainfall days and retained only those results with a relative root mean square error (RMSE) less than 0.005 and a relative inversion error less than 0.5. To avoid a high aerosol load impact, observations with a PM2.5 concentration larger than 55 μg/m^3 are also removed. Figure 2A and B present a comparison of the NO_2 concentrations at the Changjiang Middle Road and Hupo Villa sites, and the selections are made for NO_2 concentration distribution results based on MAX-DOAS UV EOP in directions 80° and 135°, respectively. The respective correlation coefficients for their comparisons are 0.659 and 0.718. This correlation coefficient is similar to other previous comparisons between near-surface NO_2 vertical profiles by MAX-DOAS and CNEMCs [35]. Meanwhile, we have also compared the NO_2 concentration obtained by the horizontal algorithm with the near-surface concentration derived from vertical profiles at azimuth 135°. Details are shown in Appendix 4 in the Supplementary Materials. Figure 2C shows the comparison results of the NO_2 concentration between the MAX-DOAS UV EOP but within the VIS EOP in directions 80° and Sanlijie sites, with a correlation coefficient of 0.532, a slope of 0.308, and an intercept of 12.171. The in situ measurements of NO_2 concentration represent the air quality near the in situ instrument, while MAX-DOAS measurements represent the average NO_2 concentration average from the observation point to the observed direction along the horizontal optical path, which is about 5 to 10 km. Therefore, the differences between the two can be understood due to this spatial distinction. Meanwhile, our MAX-DOAS instrument is mounted on a building at a height of 100 m to avoid obstructions from surrounding buildings. As a result, the NO_2 concentration information detected by the instrument is the concentration at a height of 100 m, which would probably be lower than the NO_2 concentration measured by in situ instruments located at the ground surface. The correlation between the MAX-DOAS and Sanlijie sites is lower than that for the other two CNEMC sites, which may be due to the fact that the onion-peeling method algorithm accumulates UV and VIS inversion errors simultaneously, leading to a cumulative error, as shown in Eq. 9.

Figure 3A shows the comparison of the NO_2 horizontal concentration distribution obtained by MAX-DOAS and mobile DOAS observations in Hefei from 9:00 to 11:00 on 2022 April 2. The black arrows in Fig. 3A represent the movement trajectory of the mobile DOAS. The mobile DOAS NO_2 VCD with a relative RMSE larger than 0.005 and an inversion error larger than 0.5 is filtered out. Similarly, the NO_2 VCD during the car turning time is also filtered out. Finally, 156 results of NO_2 concentration obtained from mobile DOAS observations are retained. Since there are several NO_2 VCDs obtained by mobile DOAS within each region of the ground-based MAX-DOAS results, the NO_2 results by the mobile DOAS are averaged within the area based on each region of the ground-based MAX-DOAS results. In Fig. 3A, there are a total of 18 pixel areas by MAX-DOAS covered by mobile DOAS results, and each 18 pixels encompass 3 to 18 results of NO_2 concentration data by mobile DOAS. As shown in Fig. 2D, a correlation coefficient of 0.790 is obtained between the NO_2 results measured by ground-based MAX-DOAS and mobile DOAS. Furthermore, the slope and intercept between the group results are 0.749 and 6.501, respectively. The NO_2 concentrations obtained using the two methods are consistent.

Evaluation

TROPOMI obtains the tropospheric NO_2 VCD at 13:30 (local time) (UTC+8:00). Recent studies have proved that the NO_2 VCD obtained by satellites correlates with the NO_2 concentration near the ground surface [18,36,37]. In this study, the spatial distribution of the MAX-DOAS observations between 13:00 and 14:00 is used to evaluate the satellite results. Figure 4 shows a typical NO_2 horizontal concentration spatial distribution, as observed by the satellite and MAX-DOAS instruments. Dots I and II refer to the Hefei railway and bus stations, respectively. The parallelogram pixels in Fig. 4 represent the NO_2 VCD satellite results. Only the NO_2 VCD results of the satellite pixels in the MAX-DOAS observation area are used for comparison with the NO_2 concentration results of MAX-DOAS. Figure 4 shows a similar spatial NO_2 horizontal distribution between TROPOMI and the onion-peeling method by MAX-DOAS, with the latter providing a higher resolution in the axis of NO_2 distribution. The NO_2 concentration in the northeast is higher

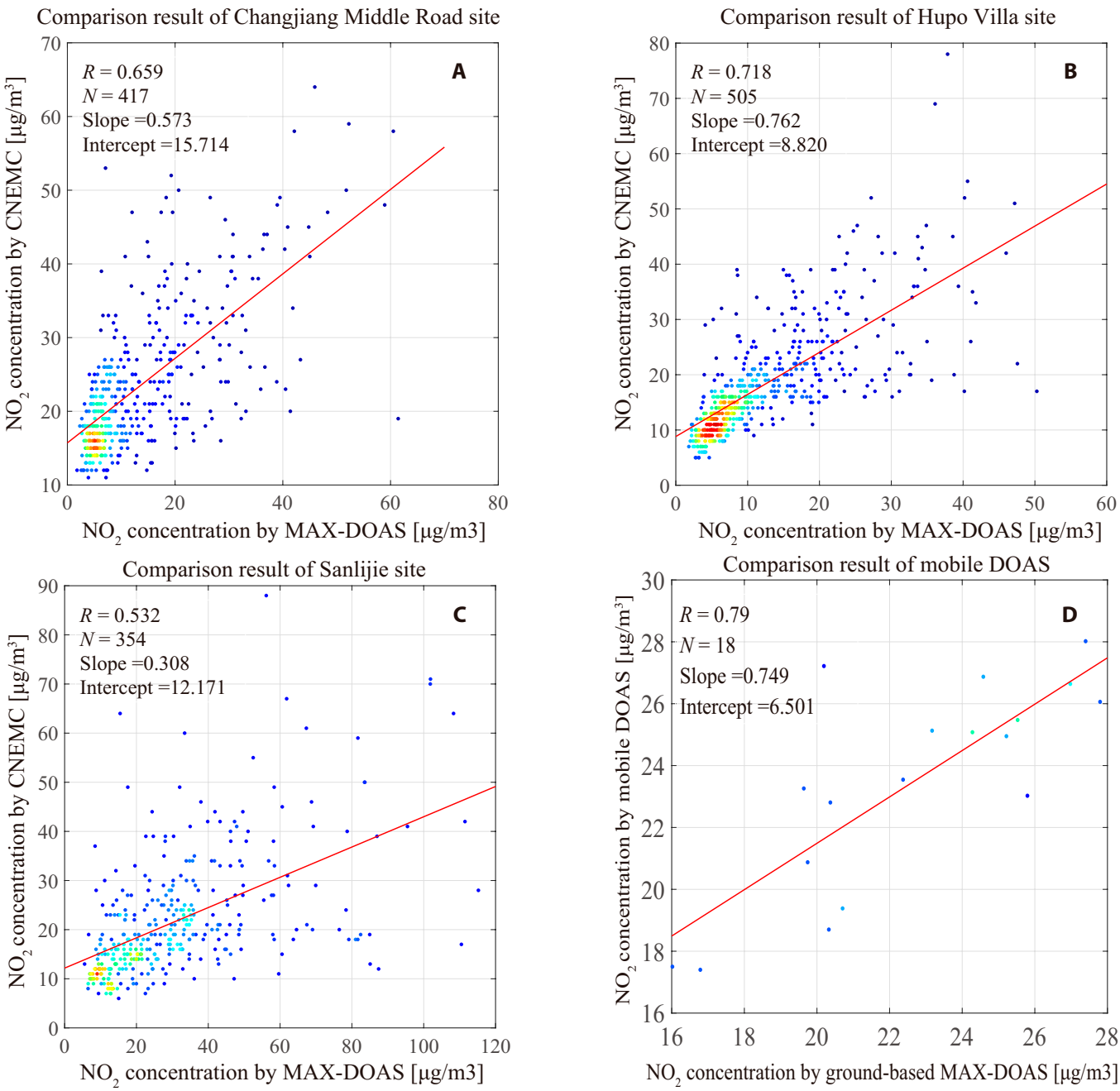

Fig. 2. Comparison of NO_2 concentrations obtained by the MAX-DOAS instrument and at CNEMCs: (A) Changjiang Middle Road, (B) Hupo Villa, and (C) Sanlijie. (D) Correlation between mobile and ground-based MAX-DOAS.

than that in the southwest. A TROPOMI pixel contains several MAX-DOAS pixels. The area of the MAX-DOAS pixel is used as the weight to obtain the weighted average corresponding to each satellite pixel. As shown in Fig. 5A, a correlation coefficient of 0.877 is obtained between the NO_2 results measured by the ground-based MAX-DOAS instrument in multiple directions and those measured by TROPOMI, and the two results are consistent.

The horizontal distribution of NO_2 obtained by the MAX-DOAS instrument, combined with the horizontal distribution of NO_2 VCD in the TROPOMI troposphere, is the most effective in determining NO_2 pollution hotspots. In the northeastern urban areas of Hefei, where the satellite NO_2 horizontal distribution concentration is relatively high, the MAX-DOAS results show that NO_2 pollution is concentrated in three small regions. The first high-value area is the UV-to-VIS optical path, which is about 6.4 to 7.4 km away from the MAX-DOAS instrument in the direction between 60° and 65°. This area is close to Hefei Xinzhan Industrial Park, which produces high levels of emissions through its intensive industrial activities. Another high-value area is identified in the UV-to-VIS optical path, which is about 5.9 to 7.1 km away from the MAX-DOAS instrument in the 75° direction, located around the Hefei railway station, which experiences high traffic flows on a daily basis. The third high-value area is the UV-to-VIS optical path, which is about 5.4 to 7.1 km away from the MAX-DOAS instrument in the

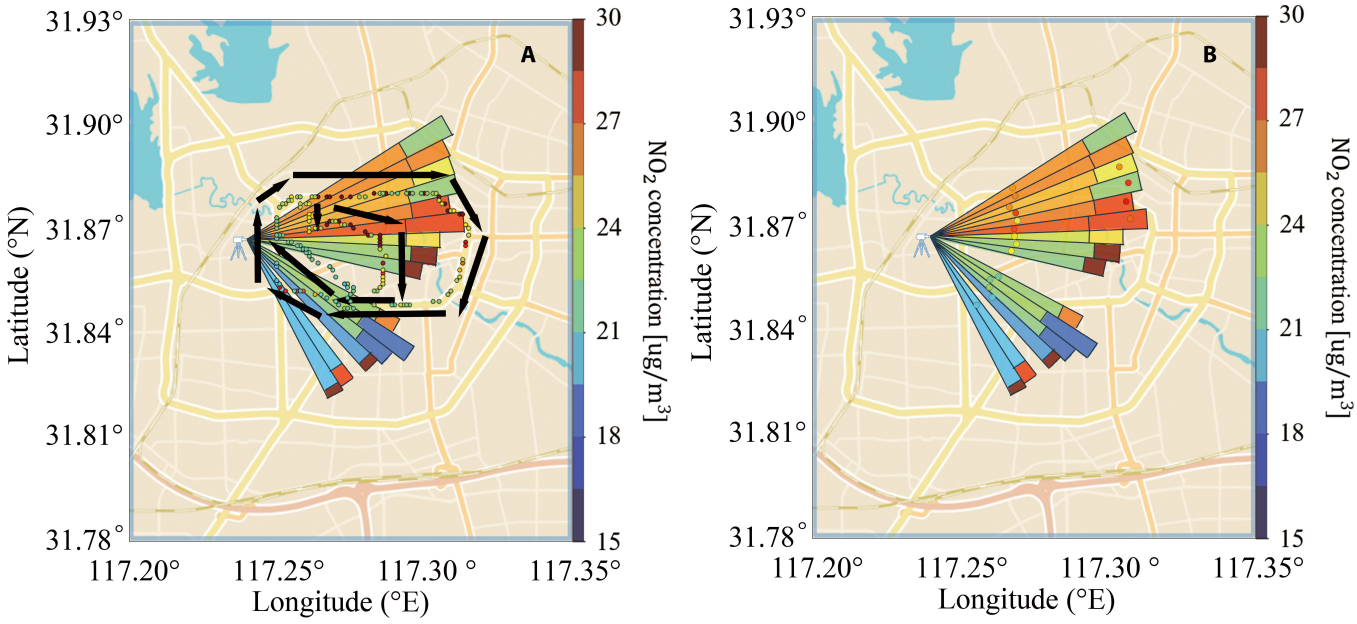

Fig. 3. Comparison of NO_2 horizontal concentration distribution observed by MAX-DOAS and mobile DOAS on 2022 April 2: (A) NO_2 concentration observed by mobile DOAS and (B) mean NO_2 concentration observed by mobile DOAS in the corresponding observed regions.

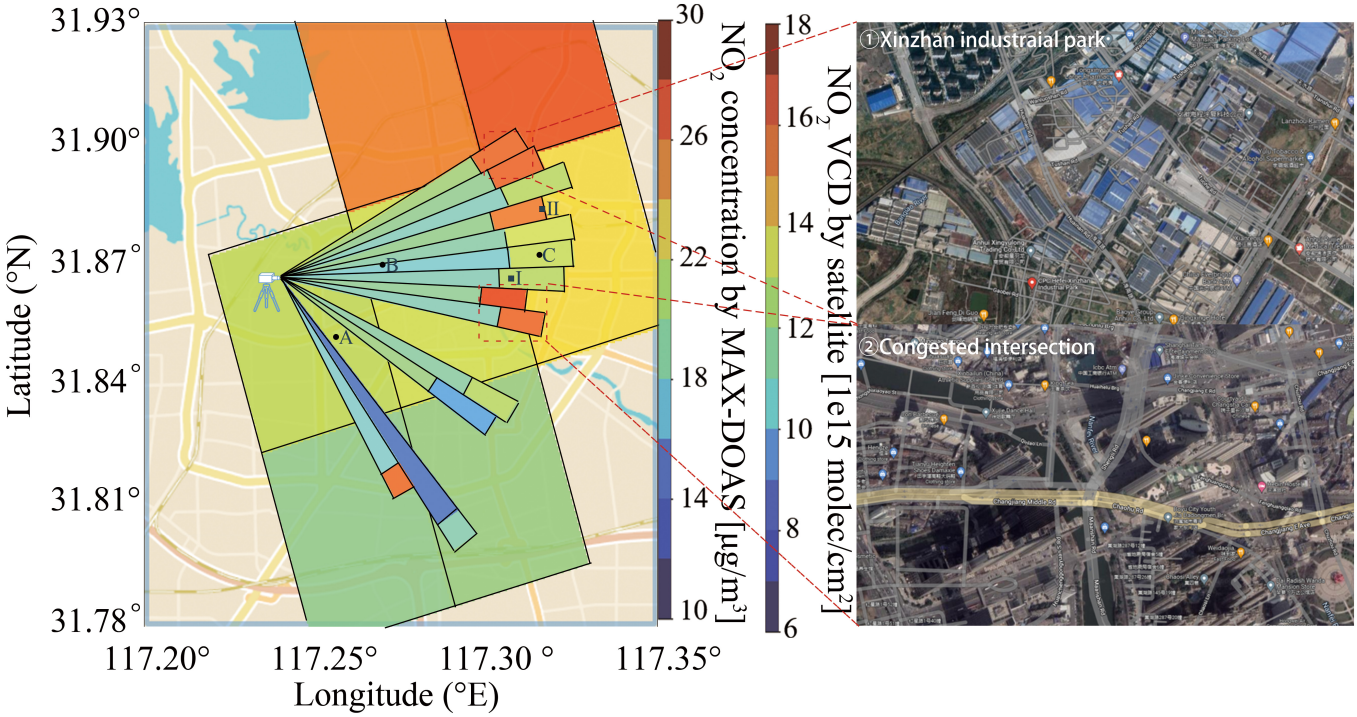

Fig. 4. Comparison of NO_2 concentration horizontal distribution observed by MAX-DOAS at 13:00 to 14:00 and NO_2 VCD by TROPOMI on 2022 April 2.

direction between 95° and 100° and primarily contains the intersection of the Yuxi Road overpass, which is an important source of pollution due to high traffic flows on working days. Overall, the onion-peeling method provided higher-resolution information in the axis than the satellite. The fourth high-value area is in the azimuth between 155° and 150° about 5.5 to 6.2 km away from the MAX-DOAS instrument. The high NO_2 concentration area is primarily located around the South Second Ring Road and the Jianghuai Automobile Manufacturing Plant. This high value of concentration could be attributed to the significant traffic volume on the South Second Ring Road. Additionally, the industrial NO_2 emissions are also a possible factor.

Satellite tropospheric NO_2 VCD has been widely used for calculating bottom-up emission and regional transmission fluxes in urban areas [38]. However, the satellite results cannot represent the daytime average concentration of NO_2 in cities.

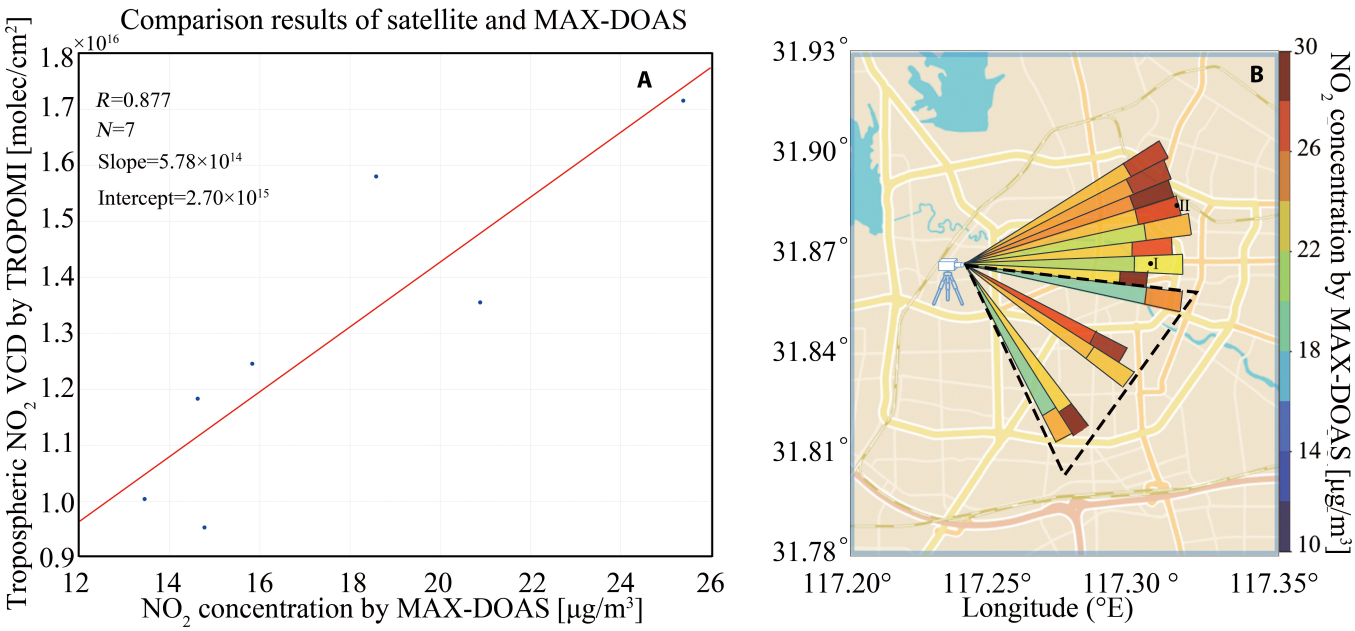

Fig. 5. (A) Correlation between TROPOMI and ground-based MAX-DOAS. (B) Daily average NO_2 concentration horizontal distribution observed by MAX-DOAS on 2022 April 2.

This is because urban NO_2 emissions are largely composed of vehicle and anthropogenic emissions during working hours. Thus, using the horizontal distribution of tropospheric NO_2 VCD obtained by satellite overpass at 13:00 (local time) makes it difficult to capture the daily variation in anthropogenic and traffic emissions in urban areas. Therefore, the emission inventory obtained from satellite data of urban areas may exhibit certain bias. To estimate this bias, the daytime average results of the NO_2 concentration obtained by MAX-DOAS are compared with hourly results between 13:00 and 14:00.

Figure 5B shows the tropospheric NO_2 VCD horizontal distribution of the daytime average NO_2 concentration determined using MAX-DOAS on 2022 April 2. When calculating the daytime average NO_2 concentration, we only select the NO_2 results derived from spectral inversions with UV and VIS EOP longer than 5 km. Meanwhile, we average the UV and VIS light paths and recalculated the NO_2 concentration results for the onion-peeling method. The concentration over the mean optical path length is the ratio of the total SCD and the total optical path length. Dots I and II are Hefei Railway Station and Hefei Bus Station, respectively. Both Hefei Railway Station and Hefei Bus Station may result in NO_2 emissions. This date represents a typical working day before China's Qingming festival holiday and has a correspondingly high flow of traffic. This is indicated by the hourly NO_2 concentrations between 13:00 and 14:00 (Fig. 5B), which are higher than that during the daytime (Fig. 4). In Fig. 4, for each pixel, the hourly NO_2 concentration between 13:00 and 14:00 is approximately 10% to 40% lower than the daytime average (Fig. 5B). One possible reason for this is that the traffic flow was lower, while the planetary boundary layer height (PBLH) is higher between 13:00 and 14:00. Therefore, the NO_2 concentration during lunch hours is not representative of the overall NO_2 concentration for that day. Because of the correlation between the NO_2 near-surface concentration and tropospheric NO_2 VCD, we can conclude that the tropospheric NO_2 VCD obtained by satellite at 13:30 (local time) on 2022 April 2 represents the daytime average tropospheric NO_2 VCD, which can lead to calculation bias.

These findings indicate that the emission inventory calculated based on the results of the satellite transit at 13:30 (local time) has certain bias due to a different underestimation of NO_2 VCDs in each pixel. To investigate this bias further, we have evaluated the bias of the results in the study area at 13:30 (local time) relative to the whole day, based on the average results within the MAX-DOAS observation period. The calculation methods for average optical path length and average results are detailed in Appendix 5 in the Supplementary Materials.

Figure 6A shows the average NO_2 horizontal distribution concentration obtained by the ground-based MAX-DOAS instrument during 2022 March 1 to 2022 May 31. A high-value region of NO_2 concentration is observed by the MAX-DOAS instrument in the azimuth from 145° to 150° and in the UV to VIS optical path in the azimuth of 60°, corresponding to the Xinzhan Industrial Park and large road networks. In the azimuth from 145° to 150°, significant traffic congestion areas, such as large roads (dot A), large shopping malls (dot B), hospitals (dot C), and the Weigang Industrial Park, may result in further NO_2 emissions. A low-value region of NO_2 concentration is observed by the MAX-DOAS instrument in the azimuth from 65° to 100° and beyond the UV optical path and within the VIS optical path in the azimuth from 105° to 140°. Pedestrian streets (square I), the Nanfei River (square II), and parks (square III) are found in the azimuth from 65° to 100°. Therefore, lower overall NO_2 emission sources are obtained. Similarly, suburban areas are found in the azimuth from 105° to 140°, with corresponding low NO_2 emissions.

Figure 6B shows the average NO_2 horizontal distribution of the satellite during the same time as in Fig. 6A, as well as the average NO_2 concentration horizontal distribution of the MAX-DOAS between 13:00 and 14:00. The overall NO_2 concentration in the UV EOP region is found to be smaller than that beyond this region but within the VIS EOP region. The horizontal distribution of NO_2 concentration shown in Fig. 6A is lower than NO_2 in Fig. 6B. The average NO_2 concentration in the daytime observation region is approximately 14.19 μg/m^3, while that in the region observed from 13:00 to

14:00 is approximately 9.86 μg/m^3. The overall NO_2 concentration in the daytime observation region is higher than the satellite transit time by approximately 42.91%. This may be due to low traffic flows and higher PBLH during 13:00 and 14:00. During this time, strong sunlight can also accelerate photolysis, resulting in decreased NO_2 emissions. The suburban area consists of the Xinzhan Industrial Park, and the Hefei railway and bus stations have relatively stable NO_2 concentrations, resulting in overall high NO_2 concentrations beyond the UV EOP region and within the VIS EOP region. Comparing Fig. 6A and Fig. 6B, the area with the largest difference between the two figures is mainly found in the direction of 60° beyond the UV EOP but within the VIS EOP and in the azimuth from 145° to 150°. Both of these directions encompass the Wulidun Interchange, South Second Ring Road, and Jinzhai Road Viaduct, constituting high-traffic areas in Hefei.

Figure 7 shows the daily variation of total NO_2 concentrations measured by MAX-DOAS in these areas and CNEMCs during the study period. Generally, the NO_2 concentration observed by the ground-based MAX-DOAS instrument and the CNEMCs is higher in the morning and gradually decreases in the afternoon. While the Hupo Villa site is located in a residential area, the Changjiang Middle Road and Sanlijie sites are located within 50 m of a road, which may cause the overall NO_2 concentration at the Hupo Villa site to be lower (Fig. 7B). As shown in Fig. 7A, the peak value of the near-surface concentration of NO_2 has occurred at approximately 9:00 and gradually decreased in the afternoon. The high NO_2 concentration in the morning could be attributed to two factors. The first is the fact that the PBLH is low in the morning, which can lead to a higher NO_2 concentration at the near-surface area. Second, mornings are characterized by high traffic flows due to rush hour, resulting in high NO_2 emissions. In the afternoon, the decrease in the overall NO_2 concentration could be attributed to the reduction of traffic flow. During the day, the increased light intensity can lead to the photolysis of NO_2 in the troposphere, resulting in the formation of ozone.

Because of its ability to cover a larger observation range, MAX-DOAS can identify areas where anthropogenic emissions have a greater impact on the daily variations in NO_2. As shown in Fig. 7A, in terms of the average NO_2 concentration distribution during the study period, the difference between the highest and the lowest daytime average in this region is 39.07%. Meanwhile, the daytime NO_2 concentration during satellite transit time is notably lower and has a difference of 40.32% between the average and the highest values. The average minimum NO_2 concentrations in the five directions during the observation period range from 33.09% to 40.85% of the maximum concentration. The maximum bias of the satellite result may be close to 69.45% compared to the day average result. As shown in Fig. 4, the NO_2 concentrations within the seven satellite pixels on 2022 April 2 show a difference ranging from 53.42% to 89.29% with the daytime average concentrations. Notably, at the southern area enclosed by the dashed line in Fig. 5B, the satellite transit time's NO_2 concentrations show even greater disparities compared to the daytime averages, suggesting that NO_2 concentrations in the south may be more influenced by anthropogenic emissions during working time. As shown in Fig. 7B, the daytime average minimum NO_2 concentrations of the Hupo Villa, Changjiang Middle Road, and Sanlijie sites during the observation period are approximately 41.62%, 42.07%, and 52.67% of the maximum concentration, respectively. Compared with in situ measurement, this technique can be used to identify areas where anthropogenic emission sources cause greater daily variations in NO_2 concentrations. In addition, the average NO_2 concentration during the observation period of the MAX-DOAS detection area that is overlapped with the three CNEMC sites was 19.92 μg/m^3. This was higher than the average NO_2 concentration of the MAX-DOAS detection area, which was approximately 14.35 μg/m^3. This indicates that the NO_2 concentrations of the CNEMC sites may result in an overestimation of the average NO_2 concentration about 40% in the main urban area of Hefei. The main reason for this overestimation could be that the CNEMC sites were too close to main roads or bus stations.

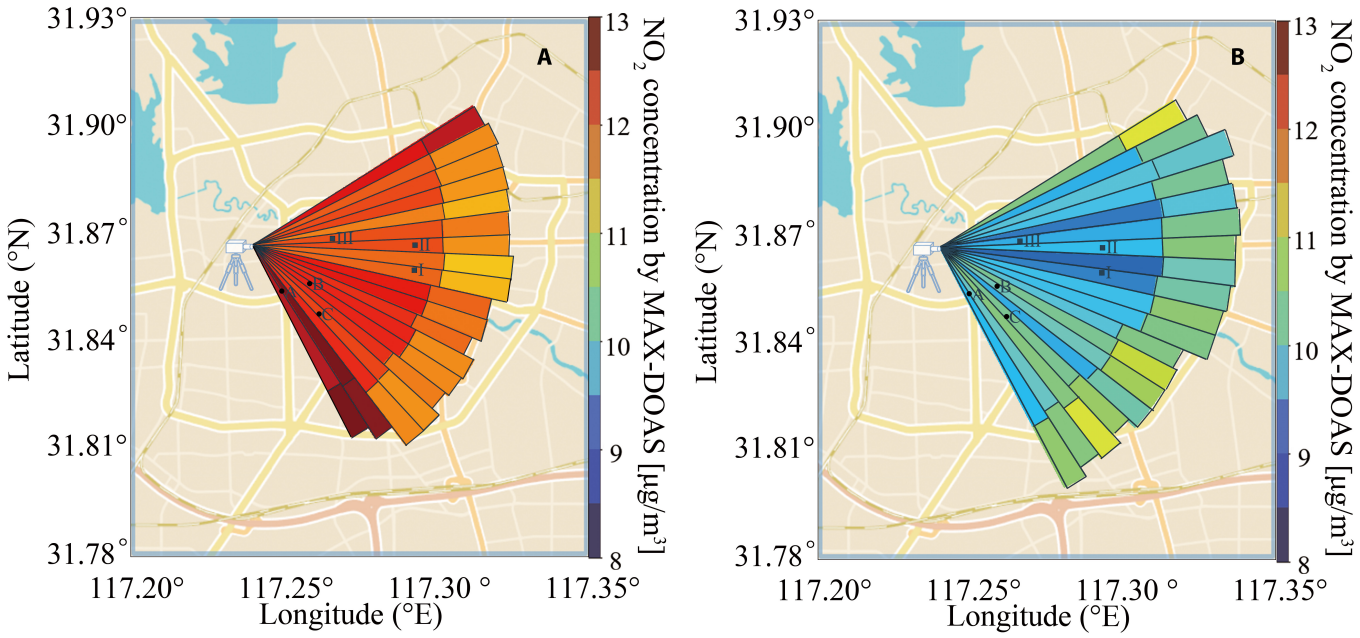

Fig. 6. Average NO_2 horizontal distribution results obtained by the MAX-DOAS instrument: (A) during the daytime and (B) between 13:00 and 14:00.

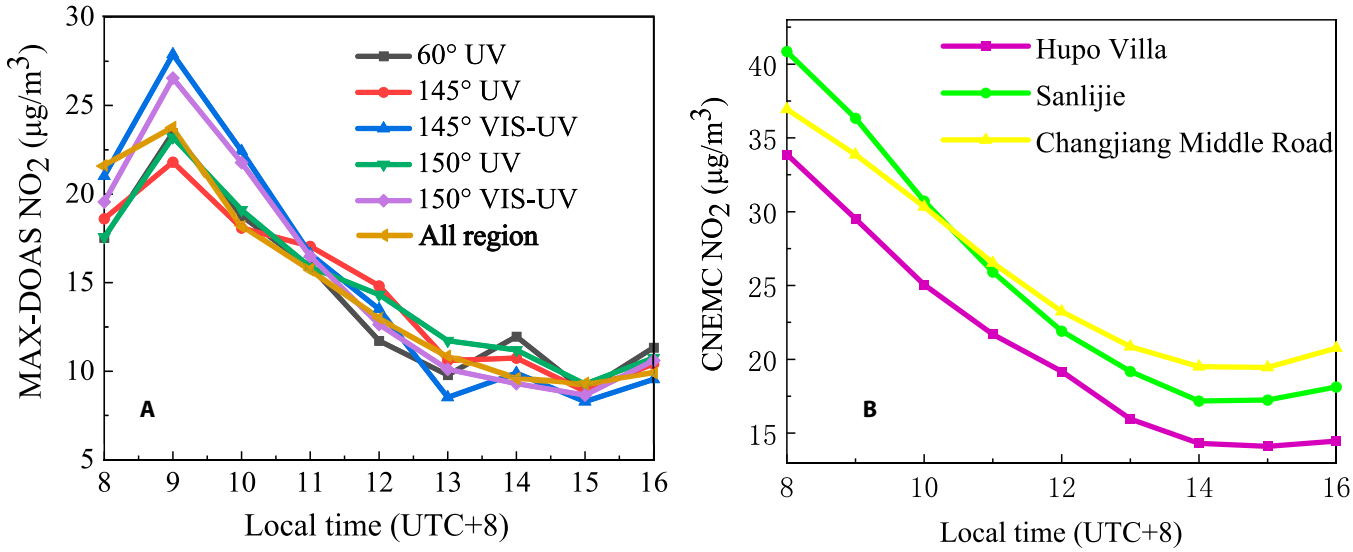

Fig. 7. Average daily variation of total NO_2 concentration: (A) MAX-DOAS and (B) CNEMCs.

Based on CNEMC data, Kong et al. [39] have reported a decrease in the NO_2 concentration of approximately 5% during 2013–2014. However, during 2013–2014, Yu et al. [10] have reported a decrease in the NO_2 VCD of approximately 13% via OMI. This indicates that the decrease of NO_2 from the CNEMC was slower. The monthly average NO_2 concentration at the three CNEMC sites decreased from 29.73 to 24.06 μg/m^3, with a decreasing rate of 19.70%. For the MAX-DOAS observations, the monthly average NO_2 concentrations decreased from 22.39 to 17.70 μg/m^3, with a decreasing rate of 22.16%. Similarly, the monthly average NO_2 VCD obtained using TROPOMI has decreased from 1.81×10^{16} to 7.2×10^{15} molecules/cm^2 for the same time period, with a corresponding rate of decrease of 60%. Taken together, these findings indicate that TROPOMI VCD has much larger decreasing rates than the CNEMC and MAX-DOAS observations. One possible reason is that the measured VCD during the overpass time of the satellite cannot accurately represent a full day of NO_2 emissions.

According to an Intergovernmental Panel on Climate Change (IPCC) report, top-down estimations of NO_x emissions from satellite retrievals of tropospheric NO_2 are strongly dependent on the choice of model and the mode retrieval, with a bias between 10% and 50% for the annual mean over polluted regions [9]. In the simulations present herein, anthropogenic emissions are assumed to be time independent. Therefore, there is a greater bias in the current satellite results. For simplicity, we have assumed that hourly factors defined the daily cycle with respect to the local time. For measurements recorded over periods shorter than 6 h, according to the literature, the daily variations that give rise to enhance the tropospheric NO_2 columns at satellite overpass times by traffic are approximately 1- to 1.2-fold overestimated [40]. Therefore, the NO_2 emissions caused by the peak traffic (i.e., 9:00), such as the observation at 145° azimuth of MAX-DOAS in this study, may result in a maximum bias of 69.45% to 83.34% in the NO_x emission inventory calculations.

Conclusions

In this study, the horizontal distribution of NO_2 is calculated based on data obtained using a ground-based MAX-DOAS instrument and the onion-peeling method for the long-term monitoring of these emissions. The corresponding results can be used to analyze the temporal and spatial variations of NO_2 in specific regions.

The results of the horizontal distribution of NO_2 calculated using a ground-based MAX-DOAS instrument are compared with several other observation methods during the study period. As a result, our NO_2 concentration results are found to be consistent with the time trend of these results for three CNEMCs. In addition, these results are consistent with the NO_2 horizontal distribution results obtained using mobile DOAS within the same period. The results obtained between 13:00 and 14:00 on a working day are also in good agreement with the TROPOMI satellite pixel results.

Following this, based on the results of the horizontal distribution of NO_2 obtained using ground-based MAX-DOAS, we have discussed the potential impact of the NO_2 VCD results of the satellite overpass at 13:30 on the calculation error of the emission source list. The emission source list is obtained by calculating the distribution results of the satellite tropospheric NO_2 VCD at 13:30 (local time) on 2022 April 2 and replacing the daily average distribution results of urban NO_2 VCD, which may not be representative because of vehicle emissions. This allows us to evaluate the tropospheric NO_2 VCD horizontal distribution of the satellite using the daytime average NO_2 concentration distribution obtained using MAX-DOAS. The results show that the hourly NO_2 concentrations obtained by MAX-DOAS in each area are 10% to 40% lower than the daily average NO_2 concentrations obtained by MAX-DOAS in these same areas on the same day.

Furthermore, we have compared the results of the average daytime horizontal distribution of NO_2 with those of the average horizontal distribution of NO_2 between 13:00 and 14:00 during the entire observational period. In general, high values are obtained by MAX-DOAS in the areas around Hefei Weigang Industrial Park in the azimuth from 145° to 150° and Xinzhan Industrial Park in the UV to VIS optical path in the azimuth of 60°. Furthermore, we evaluate regions with large deviations from the daily variations. The NO_2 horizontal distribution is highest during rush hour, according to the data obtained using MAX-DOAS. This is due to the heavy flow of traffic during rush hour, combined with the fact that there is a lower PBLH in the

morning. The lower values of NO_2 in the afternoon may be due to photolysis of NO_2 and reduced traffic emissions. Large deviations between the average minimum NO_2 concentration and daily variations during the observation period are observed (approximately 59.38% to 70.30%). Compared with the CNEMC sites, MAX-DOAS is able to observe more variable traffic areas in cities because of the higher coverage rate. The maximum bias of the satellite transit time may be close to 69.45% compared with the all-day average result, resulting in a maximum bias in the calculation of the NO_x emission inventory of approximately 69.45% to 83.34%. The measured NO_2 concentration spatial distribution obtained by MAX-DOAS is potentially useful in bottom-up emission calculation.

We expect that the technology presented in this study will help improve the assessment of areas with high anthropogenic emissions of trace gases in urban areas, as well as assist satellites in their calculation of the daily variation characteristics of trace gas emission inventories, based on the daily variation characteristics of the regions of interest.

Acknowledgments

We would like to acknowledge the DOAS UV-VIS team at BIRA-IASB led by M. Van Roozendael. We performed spectrum fitting based on QDOAS, which is a free and open-source software developed by the authors (https://uv-vis.aeronomie.be/software/QDOAS/). We also acknowledge the SCIATRAN development team at the Institute of Remote Sensing/Institute of Environmental Physics (IUP/IFE), University of Bremen. We calculated the radiation transfer model using SCIATRAN, a free and open-source software developed by them (https://www.iup.uni-bremen.de/sciatran/). We would also like to thank the CNEMC sites (Sanlijie, Hupo Villa, and Changjiang Middle Road) for providing free hourly NO_2 concentration data (http://106.37.208.233:20035/). We are also grateful for the access provided to the Copernicus Sentinel-5P Pre-operations Daily Level 2 NO_2 data [2022] processed by the Sentinel Hub (http://www.tropomi.eu/data-products/level-2-products).

Funding: This work was supported by grants from the National Science Fund for Distinguished Young Scholars (42225504); the National Key R&D Program of China (2022YFC3710101); the Anhui Provincial Natural Science Foundation (2108085-QD180); the Presidential Foundation of the Hefei Institutes of Physical Science, Chinese Academy of Sciences (YZJJ2021QN06); and the Hefei Comprehensive National Science Center, the HFIPS Director's Fund (BJPY2022B07 and YZJJQY202303).

Author contributions: C. Lu and Q.L. designed and supervised this study. C. Lu wrote the paper and Q.L. helped with the revision of the paper. C.X. and Q.H. put forward suggestions for revisions. W.T. conducted the relevant mobile DOAS experiment. H.L. assisted in figure drawing. J.L. assisted in the retrieval of ancillary data. Z.Z. and B.C. helped maintain instrument observations. C. Liu has supported this project.

Competing interests: The authors declare that they have no competing interests.

Data Availability

Publicly available datasets were analyzed in this study. These data can be found in HARVARD DATAVERSE from https://doi.org/10.7910/DVN/GAZ5P2.

Supplementary Materials

Figs. S1 to S5
Table S1

References

1. Li G, Fang C, Wang S, Sun S. The effect of economic growth, urbanization, and industrialization on fine particulate matter (PM2.5) concentrations in China. *Environ Sci Technol*. 2016;50(21):11452–11459.
2. Chen T-M, Kuschner WG, Gokhale J, Shofer S. Outdoor air pollution: Nitrogen dioxide, sulfur dioxide, and carbon monoxide health effects. *Am J Med Sci*. 2007;333(4):249–256.
3. Mohajan H. Acid rain is a local environment pollution but global concern. *Open Sci J Anal Chem*. 2018;3(5):47–55.
4. Kanaya Y, Irie H, Takashima H, Iwabuchi H, Akimoto H, Sudo K, Gu M, Chong J, Kim YJ, Lee H. Long-term MAX-DOAS network observations of NO_2 in Russia and Asia (MADRAS) during the period 2007–2012: Instrumentation, elucidation of climatology, and comparisons with OMI satellite observations and global model simulations. *Atmos Chem Phys*. 2014;14(2):7909–7927.
5. Letu H, Nakajima TY, Wang T, Shang H, Ma R, Yang K, Baran AJ, Riedi J, Ishimoto H, Yoshida M, et al. A new benchmark for surface radiation products over the East Asia–Pacific region retrieved from the Himawari-8/AHI next-generation geostationary satellite. *Bull Am Meteorol Soc*. 2022;103(3):E873–E888.
6. Li G, Fang C, Li Y, Wang Z, Sun S, He S, Qi W, Bao C, Ma H, Fan Y, et al. Global impacts of future urban expansion on terrestrial vertebrate diversity. *Nat Commun*. 2022;13(1):1628.
7. Kowalska S, Kowalski C. Effect of NO_x and NO_2 concentration increase in ambient air to daily bronchitis and asthma exacerbation, Silesian Voivodeship in Poland. *Int J Environ Res Public Health*. 2020;17(3):754.
8. Mohr C, Richter R, DeCarlo PF, Prévôt ASH, Baltensperger U. Spatial variation of chemical composition and sources of submicron aerosol in Zurich during wintertime using mobile aerosol mass spectrometer data. *Atmos Chem Phys*. 2011;11(15):7465–7482.
9. Change C. IPCC fourth assessment report. *Phys Sci Basis*. 2007;2:580–595.
10. Yu S, Yuan J, Liang X. Trends and spatiotemporal patterns of tropospheric NO_2 over China during 2005–2014. *Water Air Soil Pollut*. 2017;228(11):447.
11. Rabiei-Dastjerdi H, Mohammadi S, Saber M, Amini S, McArdle G. Spatiotemporal analysis of NO_2 production using TROPOMI time-series images and Google earth engine in a middle eastern country. *Remote Sens*. 2022;14(7):1725.
12. Zhang Y, Li Z, Bai K, Wei Y, Xie Y, Zhang Y, Ou Y, Cohen J, Zhang Y, Peng Z, et al. Satellite remote sensing of atmospheric particulate matter mass concentration: Advances, challenges, and perspectives. *Fund Res*. 2021;1(2):240–258.
13. Munro R, Lang R, Klaes D, Poli G, Retscher C, Lindstrot R, Huckle R, Lacan A, Grzegorski M, Holdak A, et al. The GOME-2 instrument on the Metop series of satellites: Instrument design, calibration, and level 1 data processing—An overview, Atmos. *Meas Tech*. 2016;9(3):1279–1301.
14. Levelt PF, Oord GHJ, Dobber MR, Malkki A, Huib V, de Johan V, Stammes P, Lundell JOV, Saari H. The ozone monitoring instrument. *IEEE Trans Geosci Remote*. 2006;44(5):1093–1101.

15. Zhang C, Liu C, Chan KL, Hu Q, Liu H, Li B, Xing C, Tan W, Zhou H, Si F, et al. First observation of tropospheric nitrogen dioxide from the Environmental Trace Gases Monitoring Instrument onboard the GaoFen-5 satellite 9. *Light Sci Appl.* 2020;9:66.
16. Veefkind JP, Aben I, McMullan K, Förster H, de Vries J, Otter G, Claas J, Eskes HJ, de Haan JF, Kleipool Q, et al. TROPOMI on the ESA Sentinel-5 precursor: A GMES mission for global observations of the atmospheric composition for climate, air quality and ozone layer applications. *Remote Sens Environ*. 2012;120(D13):70–83.
17. Zhao X, Griffin D, Fioletov V, McLinden C, Cede A, Tiefengraber M, Müller M, Bognar K, Strong K, Boersma F, et al. Assessment of the quality of tropomi high-spatial-resolution No_2 data products in the greater toronto area. *Atmos Meas Tech*. 2020;13(2):2131–2159.
18. Anand JS, Monks PS. Estimating daily surface NO_2 concentrations from satellite data—A case study over Hong Kong using land use regression models. *Atmos Chem Phys*. 2017;17:8211–8230.
19. Crippa M, Guizzardi D, Muntean M, Schaaf E, Dentener F, van Aardenne JA, Monni S, Doering U, Olivier JGJ, Pagliari V, et al. Gridded emissions of air pollutants for the period 1970–2012 within EDGAR v4.3.2. *Earth Syst Sci Data*. 2018;10(4):1987–2013.
20. Hönninger G, von Friedeburg C, Platt U. Multi axis differential optical absorption spectroscopy (MAX-DOAS). *Atmos Chem Phys*. 2004;4:231–254.
21. Schreier SF, Peters E, Richter A, Lampel J, Wittrock F, Burrows JP. Ship-based MAX-DOAS measurements of tropospheric NO_2 and S_NO in the South China and Sulu Sea. *Atmos Environ*. 2015;102:331–343.
22. Iqbal A, Ahmad N. Retrieval of NO_2 columns by exploiting MAX-DOAS observations and comparison with OMI and TROPOMI data during the time period of 2015–2019. *Aerosol Air Qual Res*. 2022;22(6):Article 210398.
23. Irie H, Takashima H, Kanaya Y, Boersma KF, Gast L, Wittrock F, Brunner D, Zhou Y, Van Roozendael M. Eight-component retrievals from ground-based MAX-DOAS observations, Atmos. *Meas Tech*. 2011;4(6):1027–1044.
24. Dimitropoulou E, Hendrick F, Pinardi G, Friedrich MM, Merlaud A, Tack F, De Longueville H, Fayt C, Hermans C, Laffineur Q, et al. Validation of TROPOMI tropospheric NO_2 columns using dual-scan multi-axis differential optical absorption spectroscopy (MAX-DOAS) measurements in Uccle, Brussels. *Atmos Meas Tech*. 2020;13(10):5165–5191.
25. Schreier SF, Richter A, Peters E, Ostendorf M, Schmalwieser AW, Weihs P, Burrows JP. Dual ground-based MAX-DOAS observations in Vienna, Austria: Evaluation of horizontal and temporal NO_2, HCHO, and CHOCHO distributions and comparison with independent data sets. *Atmos Environ: X*. 2020;5:Article 100059.
26. Dimitropoulou E, Hendrick F, Friedrich MM, Tack F, Pinardi G, Merlaud A, Fayt C, Hermans C, Fierens F, Van Roozendael M. Horizontal distribution of tropospheric NO_2 and aerosols derived by dual-scan multi-wavelength MAX-DOAS measurements in Uccle, Belgium. *Atmos Meas Tech Discuss*. 2021;2021:1–56.
27. Russell JM III, Drayson SR. The inference of atmospheric ozone using satellite horizon measurements in the band. *J Atmos Sci*. 1972;29(2):376–390.
28. Lampel J, Pöhler D, Horbanski M, Platt U. Performance of Airyx SkySpec MAX-DOAS systems during different field campaigns. *Geophys Res Abstr.* 2019;21.
29. Irie H, Kanaya Y, Akimoto H, Iwabuchi H, Shimizu A, Aoki K. First retrieval of tropospheric aerosol profiles using MAX-DOAS and comparison with lidar and sky radiometer measurements. *Atmos Chem Phys*. 2008;8(2):341–350.
30. Hong Q, Liu C, Hu Q, Xing C, Tan W, Liu H, Huang Y, Zhu Y, Zhang J, Geng T, et al. Evolution of the vertical structure of air pollutants during winter heavy pollution episodes: The role of regional transport and potential sources. *Atmos Res*. 2019;228:206–222.
31. Danckaert T, Fayt C, Van Roozendael M, De Smedt I, Letocart V, Merlaud A, Pinardi G. QDOAS software user manual. 2012.
32. Sinreich R, Merten A, Molina L, Volkamer R. Parameterizing radiative transfer to convert MAX-DOAS dSCDs into near-surface box-averaged mixing ratios. *Atmos Meas Tech*. 2013;6(6):1521–1532.
33. Seyler A, Wittrock F, Kattner L, Mathieu-Üffing B, Peters E, Richter A, Schmolke S, Burrows JP. Monitoring shipping emissions in the German bight using MAX-DOAS measurements. *Atmos Chem Phys*. 2017;17:10997–11023.
34. Wagner T, Dix B, Friedeburg C, Frieß U, Sanghavi S, Sinreich R, Platt U. MAX-DOAS O_4 measurements: A new technique to derive information on atmospheric aerosols—Principles and information content. *J Geophys Res Atmos*. 2004;109(D22):4904.
35. Xu S, Wang S, Xia M, Lin H, Xing C, Ji X, Su W, Tan W, Liu C, Hu Q. Observations by ground-based MAX-DOAS of the vertical characters of winter pollution and the influencing factors of HONO generation in Shanghai China. *Remote Sens*. 2021;13(17):3518.
36. Liu M, Lin J, Kong H, Boersma KF, Eskes H, Kanaya Y, He Q, Tian X, Qin K, Xie P, et al. A new TROPOMI product for tropospheric NO_2 columns over East Asia with explicit aerosol corrections, Atmos. *Meas Tech*. 2020;13(8):4247–4259.
37. Yin H, Sun Y, Notholt J, Palm M, Liu C. Spaceborne tropospheric nitrogen dioxide (NO_2) observations from 2005–2020 over the Yangtze River Delta (YRD), China: Variabilities, implications, and drivers. *Atmos Chem Phys*. 2022;22(6):4167–4185.
38. Liu F, van der RJ, Eskes H, Ding J, Mijling B. Evaluation of modeling NO_2 concentrations driven by satellite-derived and bottom-up emission inventories using in situ measurements over China, *Atmos Chem Phys*. 2018;18(6):4171-4186.
39. Kong L, Tang X, Zhu J, Wang Z, Li J, Wu H, Wu Q, Chen H, Zhu L, Wang W, et al. A 6-year-long (2013–2018) high-resolution air quality reanalysis dataset in China based on the assimilation of surface observations from CNEMC. *Earth Syst Sci Data*. 2021;13(2):529–570.
40. van Noije TPC, Eskes HJ, Dentener FJ, Stevenson DS, Ellingsen K, Schultz MG, Wild O, Amann M, Atherton CS, Bergmann DJ, et.al. Multi-model ensemble simulations of tropospheric NO_2 compared with GOME retrievals for the year 2000, *Atmos Chem Phys*. 2006;6(10):2943–2979.

Journal of Remote Sensing
A SCIENCE PARTNER JOURNAL

A Novel Hyperspectral Remote Sensing Technique with Hour-Hectometer Level Horizontal Distribution of Trace Gases: To Accurately Identify Emission Sources

Chuan Lu, Qihua Li, Chengzhi Xing, Qihou Hu, Wei Tan, Hua Lin, Jinan Lin, Zhiguo Zhang, Bowen Chang, and Cheng Liu

Citation: Lu C, Li Q, Xing C, Hu Q, Tan W, Lin H, Lin J, Zhang Z, Chang B, Liu C. A Novel Hyperspectral Remote Sensing Technique with Hour-Hectometer Level Horizontal Distribution of Trace Gases: To Accurately Identify Emission Sources. *J Remote Sens*. 2023;**3**:0098. DOI: 10.34133/remotesensing.0098

High spatial-temporal resolution distribution of atmospheric gaseous pollutant is an important basis for tracing its emission, transport, and transformation. Typical methods for acquiring regional atmospheric gaseous pollutant distributions are satellite remote sensing and in situ observations. However, these approaches have limitations, such as sparse overpass times for satellites and restricted coverage for in situ monitoring. In this study, we propose a method for the long-term detection of the horizontal distribution of trace gases. This method based on effective optical paths (EOPs) as the instrument's detection range. It acquires the average trace gas concentration along the EOPs by utilizing different detection distances within the ultraviolet (UV) and visible (VIS) spectral bands. Subsequently, we use the onion-peeling method to obtain trace gas concentrations at two distinct distances. The obtained trace gas horizontal distribution was consistent with the in situ and mobile measurements. Compared with satellite remote sensing, this method achieved horizontal distribution results with higher spatial and temporal resolutions, and located several small high-value areas in Hefei, China. The tropospheric NO_2 vertical column density (VCD) results of the satellite at transit time (13:30) were consistent with the hyperspectral NO_2 horizontal distribution results at 13:00 to 14:00 on the same day but were not consistent with the daily average NO_2 results. The hourly NO_2 concentration in each area was 10% to 40% lower than the daytime average obtained by the hyperspectral remote sensing result. We evaluated the errors associated with the calculation of NO_2 emissions based on the satellite results and found a bias of approximately 69.45% to 83.34%. The spatial distribution of NO_2 concentration obtained from MAX-DOAS measurements may help in future bottom-up emission calculations.
Image

Journal of Remote Sensing (ISSN 2694-1589) is published by the American Association for the Advancement of Science. 1200 New York Avenue NW, Washington, DC 20005.